Lateral redistribution of heat and salt in the Nordic Seas

Michael A. Spall [a],[*], Mattia Almansi [b],[c], Jie Huang [a], Thomas W.N. Haine [c], Robert S. Pickart [a]

[a] Woods Hole Oceanographic Institution, Woods Hole, MA, United States
[b] National Oceanography Centre, Southampton, United Kingdom
[c] Johns Hopkins University, Baltimore, MD, United States

A B S T R A C T

The locations, times, and mechanisms by which heat and salt are transported through and within the Nordic Seas are discussed. The analysis is based on a regional, high resolution coupled sea ice-ocean numerical model, a climatological hydrographic data set, and atmospheric reanalysis. The model and climatology are broadly consistent in terms of heat loss, water masses, and mean geostrophic currents. The model fields are used to demonstrate that the dominant exchange between basins is an export of warm, salty water from the Norwegian Sea into the Greenland and Iceland Seas, with both the mean cyclonic boundary current system and eddy fluxes playing important roles. In both the model and the climatology, approximately 2/3 of the heat loss to the atmosphere over the Nordic Seas is found over the mean cyclonic flow and 1/3 takes place within the closed recirculations in the interior of each of the basin gyres, with the Norwegian Sea having the largest heat loss. The seasonal cycle is dominated by local air-sea heat flux within the gyres while it is dominated by lateral advection in the cyclonic boundary current, particularly in the northern Norwegian and Greenland Seas. The freshwater flux off the east Greenland shelf is correlated with the local winds such that in winter, when winds are generally towards the southwest, freshwater is advected onto the shelf and in summer, when winds are weak or towards the northeast, freshwater is advected into the Greenland Sea, which leads to salinification in winter and freshening in summer.

1. Introduction

The Nordic Seas refers to the collection of basins that lie between the Greenland-Scotland Ridge to the south and Fram Strait between Greenland and Svalbard to the north. The Barents Sea is sometimes considered as part of the Nordic Seas (e.g., Hansen and Østerhus, 2000), but for our analysis we consider only the Norwegian, Greenland, and Iceland Seas (Fig. 1). Approximately 8 Sv (1 Sv = 10^6 m^3 s^{-1}) of relatively warm, salty water flows northward from the eastern subpolar North Atlantic into the Norwegian Sea (Mauritzen, 1996b; Hansen and Østerhus, 2000; Østerhus et al., 2019). This water progresses poleward in two separate currents (Orvik and Niiler, 2002): the Norwegian Atlantic Slope Current along the Norwegian coast and the Norwegian Atlantic Front Current offshore over the Mohn-Knipovich Ridge. There is also a comparatively small transport (1–2 Sv) by the North Icelandic Irminger Current along the west coast of Iceland into the Iceland Sea (Jónsson and Valdimarsson, 2012; Casanova-Masjoan et al., 2020:). After crossing Denmark Strait, roughly half of this current recirculates back to the Irminger Sea while the remainder merges with the East

Icelandic Current north of Iceland (Casanova-Masjoan et al., 2020:).

The circulation within the Nordic Seas is strongly coupled with the bottom topography (Vöet et al., 2010). It is dominated by a baroclinic cyclonic boundary current system and more barotropic cyclonic recirculation gyres over each deep basin. The existence of these gyres was originally inferred by Helland-Hansen and Nansen (1909), and later confirmed by several studies based on surface drifters (e.g., Poulain et al., 1996:; Orvik and Niiler, 2002; Jakobsen et al., 2003) and sparse deep water measurements (Hansen and Østerhus, 2000). The boundary current in the eastern basin (Norwegian Atlantic Slope Current) splits at the Barents Sea opening with approximately 2 Sv flowing into the Barents Sea (Ingvaldsen et al., 2002) and the remainder flowing northward as the West Spitsbergen Current. Roughly half of this transport recirculates near Fram Strait while the rest enters the Arctic Ocean and circumnavigates the different basins before exiting the Arctic Ocean through Fram Strait and the Canadian Arctic Archipelago. The southward flow through Fram Strait, along with a small fraction of Pacific-origin Water (Woodgate et al., 2006, 2012) and recirculated Atlantic Water, forms the East Greenland Current that flows equatorward along
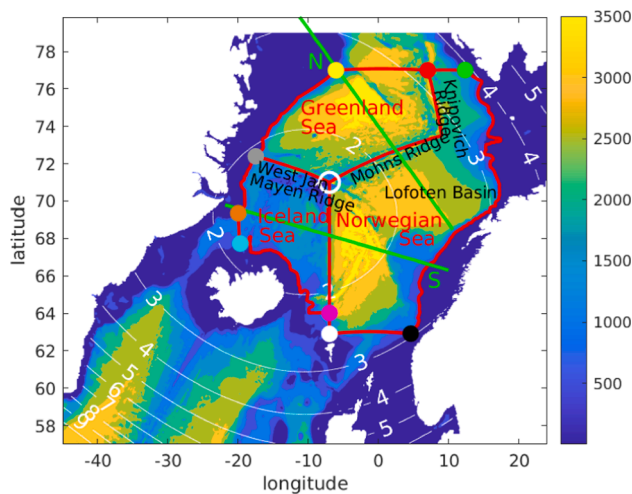
Fig. 1. Bottom topography (in meters) with sections defining the Norwegian Sea, Greenland Sea, and Iceland Sea basins. The colored circles indicate the locations of the section ends to be used later. The white contours indicate the horizontal grid spacing of the model (km). The green lines mark the locations of the southern and northern hydrographic sections discussed below.

the western boundary of the Nordic Seas.

Along this cyclonic loop through the Nordic Seas and Arctic Ocean the warm, salty Atlantic Water is cooled by lateral mixing and heat loss to the atmosphere, and freshened by river runoff, precipitation, and the Pacific Water emanating from Bering Strait. Although the largest heat loss occurs over the broad, relatively warm Norwegian Sea, the densest waters are found within the closed recirculation gyres that lie over the deep basins in the Greenland and Iceland Seas. Early analysis pointed to these regions as the locations for the formation of the dense waters that overflow through Denmark Strait and the Faroe-Bank Channel (Swift et al., 1980; Aagaard et al., 1985; Strass et al., 1993). Subsequent studies emphasized the role of the cyclonic boundary current system in the bulk of water mass transformation (Mauritzen, 1996a,b; Eldevik et al., 2009). It is now known that the densest overflow waters in the Denmark Strait are supplied by the North Icelandic Jet, which originates over the north slope of Iceland (Jónsson and Valdimarsson, 2004; Våge et al., 2011, 2013; Semper et al., 2019), while the Faroe Bank Channel overflow is fed by the Iceland-Faroe Slope Jet flowing eastward along the north side of the Iceland-Faroe Ridge (Semper et al., 2020). The hydrographic properties of both currents suggest that the waters were last in contact with the atmosphere in the central Greenland Sea (Huang et al., 2020). Brakstad et al. (2019) estimated that the intermediate water mass formed by convection in the Greenland Sea accounts for at least 20% of both the North Icelandic Jet and the Faroe-Bank Channel Overflow.

Heat loss in the Nordic Seas is much larger compared to the subpolar North Atlantic between Greenland and Scotland, and the Labrador Sea combined (Chafik and Rossby, 2019). Therefore, water mass transformation within the Nordic Seas plays a central role in the downwelling limb of the meridional overturning circulation, both in density space and in depth space. A total of roughly 5.5 Sv of dense overflow water, the main source for North Atlantic Deep Water (Dickson and Brown, 1994), leaves the Nordic Seas east and west of Iceland. The two major overflows pass through Denmark Strait (3.2–3.5 Sv; Harden et l., 2016; Jochumsen et al., 2017; Lin et al., in press) and the Faroe-Bank Channel (∼ 2 Sv; Borenäs and Lundberg, 2004; Hansen et al., 2016; Østerhus et al., 2019). Turbulent entrainment just downstream (south) of the Greenland-Scotland Ridge roughly doubles these overflow transports while reducing their density anomaly relative to the ambient water (Price and Baringer, 1994; Dickson and Brown, 1994). The northward flow of warm water and southward flow of cold water reflects the net meridional heat transport by the cyclonic current system that flows through the Nordic Seas. Part of this overturning is in the vertical (warm, northward

shallow; cold, southward deep) and part is in the horizontal (warm, northward in the east; cold, southward in the west). This northward heat transport is important for the regional climate (Oliver and Heywood, 2003) and also keeps much of the Nordic Seas ice-free to a higher latitude than in the Pacific Ocean, enhancing air-sea exchange in winter. Variability in heat transport through the Nordic Seas also influences the surface air temperature, geostrophic winds, and ice extent in the region on interannual (Schlochtholz, 2013) and decadal (Årthun and Eldevik, 2016) time scales.

Most prior studies of the heat and freshwater budgets in the Nordic Seas have focused on where heat is lost to the atmosphere (e.g., Mauritzen, 1996a,b; Simonsen and Haugan, 1996; Segtnan et al., 2011; Latarius and Quadfasel, 2016). While this is clearly important, our interest is not only where the heat is lost but also how heat and salt are advected from the inflows in the south and north to the individual basins and gyres. We combine analysis of a high-resolution regional model of the Nordic Seas with a climatological hydrographic data base and atmospheric reanalysis products to estimate the relative influences of air-sea exchange and mean and eddy lateral advection between basins as a function of depth and time.

2. A regional model of the Nordic Seas

We set up a high-resolution, realistic general circulation model of the Nordic Seas. The dynamics are simulated using the Massachusetts Institute of Technology General Circulation Model (MITgcm; Marshall et al., 1997). The model solves the hydrostatic Navier-Stokes equations under the Boussinesq approximation for an incompressible fluid with a nonlinear free surface (Campin et al., 2004). The equation of state by McDougall et al. (2003) and the K-profile parameterization (KPP; Large et al., 1994) are implemented. The ocean model is coupled with the MITgcm sea ice model (Losch et al., 2010).

The model domain (Fig. 1) covers a larger area compared to previous configurations targeting Denmark Strait (Almansi et al., 2017, 2020). It includes the entire Iceland, Greenland, and Norwegian Seas. The numerical domain is discretized with an unevenly-spaced rectilinear grid. The horizontal resolution is about 2 km over the Iceland Sea and decreases moving toward the edges of the domain. The lowest resolution in the region of interest for this study is about 4 km. The bathymetry is obtained from RTopo-2.0.4 (Schaffer et al., 2019:) and is accurately represented by partial bottom cells. The vertical grid uses the re-scaled height coordinates z^* (Adcroft et al., 2004). The vertical resolution at rest linearly increases from 2 to 19 m in the upper ∼ 200 m and is 19 m thereafter.

After an 8-month spin up starting in January 2017, we stored the numerical solutions from September 2017 to August 2018 every 6 h. This time period encompasses the Iceland Greenland Seas Project (IGP), an atmosphere-ocean field campaign carried out in February–March 2018 to investigate the ventilation of dense water in the western Nordic Seas (Renfrew et al., 2019). The model solutions are publicly available on the Johns Hopkins SciServer system (Medvedev et al., 2016). Additional fields, such as the tendency terms for tracer budgets, have been computed using OceanSpy v0.1 (Almansi et al., 2019).

The initial conditions for the oceanic component are obtained from HYCOM + NCODA GOFS 1/12° Analysis (Cummings, 2005; Cummings and Smedstad, 2013; Helber et al., 2013), whereas the sea ice fields are initialized using the TOPAZ4 reanalysis (Xie et al., 2017). The products used to initialize the model also provide the lateral boundary conditions (3-hourly and daily frequency for the oceanic and sea ice fields, respectively). Sea surface temperature is relaxed with a 10-day timescale to the global analysis OSTIA (Donlon et al., 2012). The surface heat flux in the Nordic Seas is in general 1–3 orders of magnitude larger than this relaxation heat flux and so it does not have a significant influence on the present analysis.

The oceanic and sea ice components are forced at the surface with heat, freshwater, and momentum fluxes derived from the atmospheric

reanalysis ERA5 (Copernicus Climate Change Service (C3S), 2017). The bulk fluxes are computed using hourly air temperature and specific humidity at 2 meters height, downward shortwave and longwave radiation, solid and liquid precipitation, evaporation, and wind velocities at 10 meters height.

3. Hydrographic climatology of the Nordic Seas

Historical hydrographic data from 2013 to 2018 were used to construct the climatology of hydrographic sections in the Nordic Seas used in the study. The majority of the data were obtained from the Unified Database for Arctic and Subarctic Hydrography (UDASH). Additional data outside the time period and spatial domain of UDASH, come from various archives (see Huang et al., 2020, for the description of individual data sources). In addition to the quality control already performed on each data source, duplicates between the different archives were removed. Data outside the expected range in the Nordic Sea [-2–$20\,°C$ for potential temperature, 20–36 for practical salinity] and data with density inversion exceeding 0.05 kg m^{-3} were excluded. Additional details of the final combined dataset are provided in Huang et al. (2020).

The composite vertical sections of temperature and salinity discussed in the following section were constructed from profiles with lateral distances less than 50 km from the selected line, using Laplacian-spline interpolation (Pickart and Smethie, 1998). The positions of profiles along the section were determined by the distance between their projected location and the origin of the section (the western boundary). The resulting climatological vertical sections have a horizontal resolution of 25 km and a vertical resolution of 50 m.

As the coverage of hydrographic data over 2013–2018 is not sufficient to construct gridded dynamic height in the Nordic Seas, the climatology of dynamic height (1986–2018) from Huang et al. (2020) was used to determine the locations of Greenland Sea and Iceland Sea gyres (the out-most closed contours of surface dynamic height relative to 500 m). The relative geostrophic velocities referenced to the sea surface were computed from the dynamic height field. The absolute geostrophic velocities were obtained by using satellite-derived mean surface geostrophic velocity from 1993 to 2018 as the reference, which can be accessed at Copernicus Marine Environment Monitoring Service (CMEMS).

4. Mean hydrography, circulation, and seasonal cycle

The basic hydrographic structure and circulation in the Nordic Seas are briefly presented. The Nordic Seas have been divided into three regions: the Norwegian Sea; the Greenland Sea; and the Iceland Sea. These regions are largely defined by the bottom topography and the northern and southern limits of the basin. Fig. 1 shows the bottom topography and the boundaries defining the three basins. The coastal limit of the basins is defined as the 650-m isobath, roughly in accord with the sill depth in Denmark Strait. The northern limit is placed at 77 °N, just north of the deepest part of the Greenland Sea. The southern limit of the Norwegian Sea is 62.9 °N, just south of the deepest part of the Norwegian basin. The western limit of the Iceland Sea is at 20 °W, just west of the Kolbeinsey Ridge. Within the Nordic Seas, the Norwegian Sea is separated from the Greenland Sea by the Mohn Ridge and from the Iceland Sea by the eastern edge of the Iceland Plateau. The boundary between the Greenland Sea and the Iceland Sea is approximately the West Jan Mayen Ridge.

4.1. Hydrography

The mean temperature and salinity are presented along two sections that cross the Nordic Seas, one to the south through the Iceland Sea and one to the north through the Greenland Sea (Fig. 1). These are two of the transects analyzed by Huang et al. (2020). These model sections have

been interpolated to the same horizontal and vertical grid as was used in the climatological hydrography. The reader should keep in mind that the model depicts 2017–18, whereas the observations represent a 2013–2018 climatology that is biased towards more sampling during the summer and fall. However, the main point of this comparison is not a detailed evaluation of the model for that year but rather a demonstration that the model represents the dominant hydrographic features on the basin scale, which are always present.

The southern section is dominated by warm, saline water along the eastern boundary, associated with the inflow of subtropical-origin water into the Nordic Seas (Fig. 2). This warm, salty water extends towards the west until it encounters the Jan Mayen Ridge separating the Iceland and Norwegian Seas. The thermocline in the Norwegian Sea is located at approximately 600 m depth, with cold, weakly stratified water below. This depth is approximately set by the sill depths to the south (Spall, 2010). The model is slightly cooler and fresher than the climatology, likely related to cold, low salinity water fluxed off the north Icelandic shelf into the southern Norwegian Sea. Although there is observational evidence for such an exchange (Perkins et al., 1998), it appears to be too strong in the model. There is a strong baroclinic front located over the Jan Mayen Ridge where the thermocline rises to near the surface in both the model and the climatology. This is the hydrographic signature of the Norwegian Atlantic Front Current. There is also warm and salty water banked up against the east coast of Greenland, associated with the East Greenland Current, although in the model this water is slightly warmer, fresher, and deeper than in the climatology. There is also very cold and fresh polar-origin water located over the east Greenland shelf.

The section to the north shows similar features (Fig. 3). The Norwegian Sea is dominated by a warm, salty upper ocean, a thermocline around 700 m depth, and a weakly stratified, cold and fresh Greenland Sea. The model is more stratified in the middle of the Greenland Sea than in the Iceland Sea. In the Norwegian Sea the model thermocline is a little cooler, fresher, and shallower than the climatology. Some of the difference in the Greenland Sea may be attributed to the relatively mild winter in 2017/2018, which would not be reflected fully in the 5 year climatological mean. Unfortunately, there was not sufficient data coverage during that winter to construct hydrographic sections.

4.2. Circulation

The depth integrated transport streamfunction from the model, from the surface to 692.5 m, reflects the topographic features that define the basins (Fig. 4). The circulation is dominated by a cyclonic rim current and closed cyclonic gyres within each basin. The northward flow in the Norwegian Atlantic Slope Current along the eastern boundary is about 7 Sv, on par with the observed mean transport of 5.2 Sv (Mauritzen et al., 2011; Orvik et al., 2001). The maximum transport of the cyclonic gyre in the Norwegian Sea is approximately 6 Sv. The closed anticyclonic Lofoten Eddy is also evident, with a mean transport of approximately 12 Sv. Approximately 5 Sv flows northward to Fram Strait along the eastern boundary, into the Arctic, and returns southward along the western boundary. The Greenland Sea exhibits a large region of closed cyclonic recirculation with maximum transport of 3 Sv. Of the remaining 5 Sv flowing southward along the western boundary of the Greenland Sea, approximately 3 Sv continues to the south along the boundary and 2 Sv flows to the east just to the north of the Jan Mayen Ridge (forming the Jan Mayen Current) to eventually exit the domain to the east of Iceland. Within the Iceland Sea there is a small cyclonic gyre with 3 Sv transport. There is also a loss of about 1 Sv from the East Greenland Current in the southern Iceland Sea, forming the East Icelandic Current.

In general, the Nordic Seas are characterized by a northward flow of warm, salty water into the Norwegian Sea, an export of cooler, fresher water to the Arctic Ocean, an import of colder and even fresher water from the Arctic Ocean, and an export of both this cold, fresh Arctic-origin Water and the cooler, fresher remnants of Atlantic-origin Water to the south. The Nordic Seas are a region of heat loss and freshwater
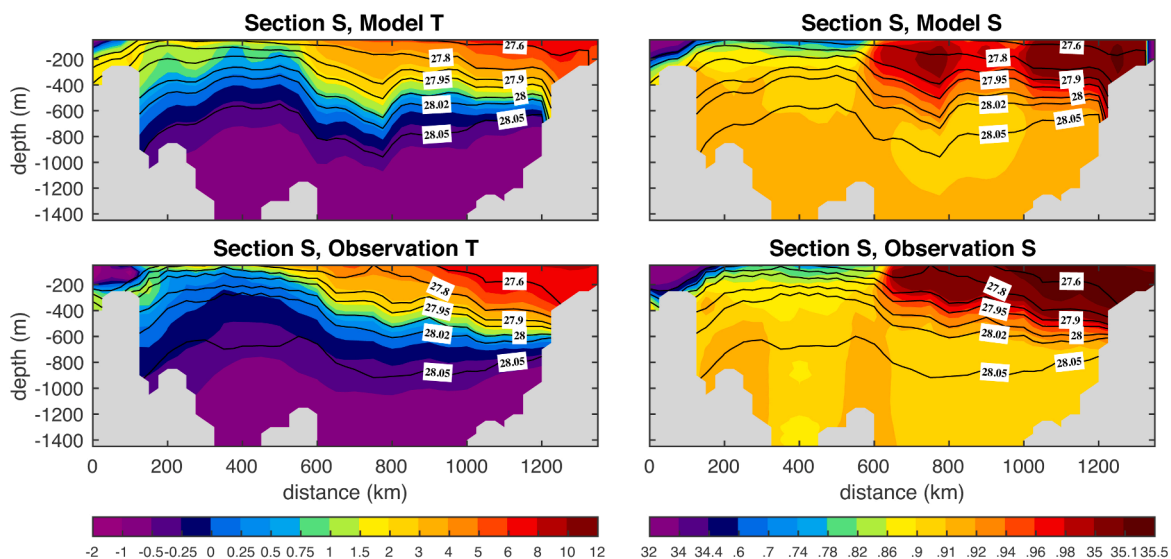
Fig. 2. Sections of the model and climatological temperature (color, °C) and salinity (color, psu) along the southern section from the Norwegian Sea across the Iceland Sea in Fig. 1. The black contours are potential density (kg m^{-3}).
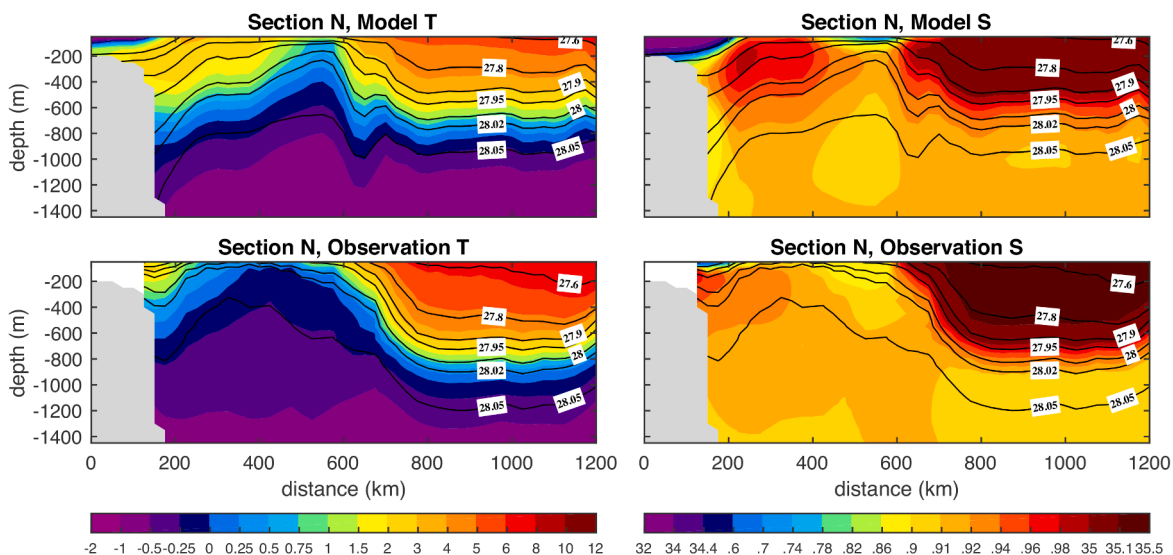

Fig. 3. Same as Fig. 2 except for the northern section from the Norwegian Sea across the Greenland Sea in Fig. 1.

gain. The surface buoyancy forcing is dominated by the heat flux, as the net evaporation minus precipitation contributes relatively little to the densification and water mass transformation by air-sea fluxes.

The three basins are characterized by regions of closed mean recirculations and a cyclonic boundary current. The closed gyres in the model are defined by the outermost closed transport contour within each basin, indicated by the yellow lines in Fig. 4. Within these closed gyres the heat loss is balanced by lateral eddy fluxes from the cyclonic flow. Heat loss from the boundary currents, through these lateral eddy fluxes and by direct atmospheric forcing, is balanced by mean advection. The relative importance of the closed gyres and the cyclonic circulation to the total heat exchange with the atmosphere is indicated by the integrated surface heat flux within each region shown in Table 1. 55% of the heat loss in the model Nordic Seas occurs in the Norwegian Sea, 35% occurs in the Greenland Sea, and only about 10% of the total heat loss occurs in the Iceland Sea. Within each basin, the heat loss outside the region of closed gyres is larger than that within the closed gyres, especially for the Norwegian and Iceland basins. Overall, heat loss from within the gyres accounts for about 1/3 of the total heat loss and the remaining 2/3

occurs outside the gyres, primarily in the cyclonic boundary current. This is consistent with the dominant role of the cyclonic boundary current in water mass transformation proposed by Mauritzen (1996a).

Analysis of the climatological ERA5 surface heat fluxes for the same IGP year as the model run yields a similar result, where the gyres are identified using the hydrographic climatology (Table 1). In particular, in the Greenland and Iceland Seas the gyres are defined by regions of outermost closed surface dynamic height (relative to 500 m). As there are no closed surface dynamic height contours in the Norwegian Sea, a transport streamfunction of absolute geostrophic velocity over the upper 700 m was calculated from the sea surface height field and the thermal wind derived from the dynamic height, which results in a closed cyclonic recirculation gyre in the Norwegian Sea, as also seen in the model. (The locations of these closed gyres is indicated in Fig. 6b, d.) This points to the importance of the deep cyclonic circulation in the Norwegian Sea. The climatology indicates more total heat loss over the entire Nordic Seas ($8.2 \times 10^{13} W$ compared to $6.6 \times 10^{13} W$ in the model) with 72% occurring in the Norwegian Sea, 22% in the Greenland Sea, and 6% in the Iceland Sea. The lower heat loss in the model Norwegian Sea is due
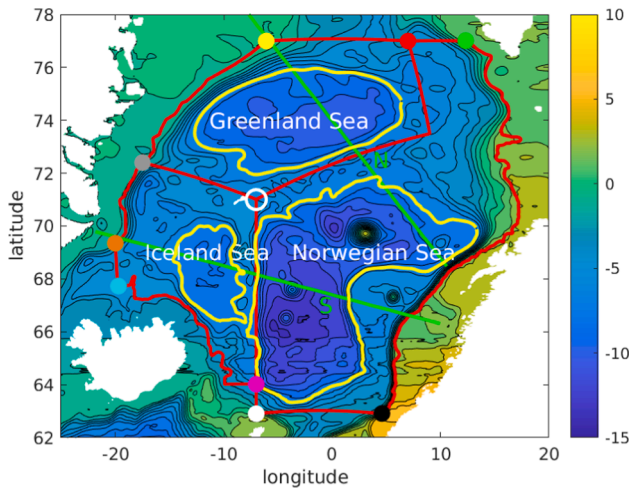
Fig. 4. Mean model transport streamfunction (Sv, surface to 692.5 m depth) in the Nordic Seas. The contour interval is 1 Sv and the yellow contour is the outer-most closed contour within each basin. The green lines mark the locations of the southern and northern hydrographic sections shown in Figs. 2, 3.The colored circles indicate the locations of the section ends to be used later.

to the surface cold bias in the model. The observations also show a dominance of the regions outside the closed gyres compared to the heat loss within the closed gyres. The most significant difference is in the lesser importance of the Greenland Sea gyre in the observations, which may in part be due to the smaller region of closed recirculation compared to that in the model. While the total heat fluxes and their distribution are somewhat different, the overall message is the same: most of the heat loss occurs in the Norwegian Sea and the cyclonic boundary current accounts for approximately twice as much heat loss as the regions of closed recirculations.

4.3. Seasonal evolution

The seasonal evolution of the basin-averaged temperature and salinity over the upper 692.5 m in the model is shown in Fig. 5. This is an average over the regions defined by the red lines in Fig. 1. The seasonal cycle in temperature is dominated by heating in summer and cooling in winter. The heat loss in winter results in convective overturning that is deepest within the closed gyres in the interior of the basins. Convection reaches 800 m in the Greenland Sea Gyre and 400 m in the Iceland Sea Gyre. By way of comparison, using 30 years of data Brakstad et al. (2019) found mean wintertime mixed layer depths in the central Greenland Gyre to be order 500 m. However, the climatology used here indicates that, for individual profiles, mixed layers can exceed 1500 m. Long-term average winter mixed layers in the Iceland Sea Gyre are observed to be order 150 m (Vage et al., 2015), while our climatology reveals that individual mixed layers can exceed 300 m. In the model, the deepest convection events are found on relatively small scales of 10's of kilometers and hence are not evident in the basin-averaged hydrography. There is also convection extending down to 800 m in the Norwegian

Sea, but these events are isolated within relatively light-density anti-cyclonic eddies and do not represent the formation of dense waters that contribute to the dense overflows. In summer, the regions of deep convection in the Greenland and Iceland Seas are restratified by a combination of atmospheric heating and lateral eddy advection. Each of the basin averages shows a similar pattern of warming and freshening in the upper 100 m in summer, followed by cooling and convective mixing over the upper 200–300 m in winter. Each of the basins also shows a change in the water properties throughout the water column over the year of the model simulation: The Norwegian Sea becomes cooler and fresher, while the Greenland and Iceland Seas become warmer with little trend in salinity below the upper 100 m. In the upper 200 m the seasonal evolution is much larger than the trend but below this depth the trend exceeds the seasonal evolution. These deep trends are unique to this specific year of integration, 2017–2018. Other model runs with similar configurations but forced with reanalysis from different time periods do not produce such trends (Almansi et al., 2017, 2020).

The relative importance of advection to local surface fluxes in the seasonal restratification is characterized by the ratio of the magnitude of the annual mean heat loss to the atmosphere to the heat input into the ocean ($Q > 0$) during the heating season, which we call Q_R.

$$Q_R = \frac{|\int Q \, dt|}{\int \mathcal{H}(Q) Q \, dt} = \frac{|\overline{Q}|}{Q^+}, \tag{1}$$

where $\mathcal{H}$ is the Heaviside step function, defined as $\mathcal{H}(Q) = 1$ for $Q \geqslant 0$ and $\mathcal{H}(Q) = 0$ for $Q < 0$. This allows for a measure of the importance of oceanic advection based solely on the surface heat flux. For $Q_R \ll 1$ the amount of surface heat loss in winter is close to the amount of heat gain in summer and so the seasonal cycle is dominated by local air-sea exchange and advection is not very important for restratification. However, when $Q_R \gg 1$ the amount of heat gain in summer can not compensate for the large heat loss in winter and thus oceanic advection must be important. This analysis of course assumes that the heat budget is closed over the mean annual period.

The annual mean surface heat flux in the model is shown in Fig. 6a, where negative values indicate heat is lost to the atmosphere. There is cooling over most of the Nordic Seas with the strongest heat loss over the cyclonic boundary current and in the Norwegian Sea (again consistent with Mauritzen (1996a)). The model shows a net heat gain just north of Iceland and over the Iceland-Faroe ridge. This is related to the cold, fresh water that flows from the north shelf of Iceland to the east along the Iceland Faroe Ridge, resulting in a cold surface bias in the model and too much heat uptake by the ocean. The ratio Q_R (Fig. 6c) shows that seasonal restratification due to lateral advection is an order of magnitude larger than local heating in the northern Norwegian and Greenland Seas, particularly along the cyclonic boundary current. On the other hand, local heating is more important than advection for seasonal restratification in the Greenland and Iceland Sea gyres and in the southern Norwegian Sea.

The same quantities calculated from the ERA5 reanalysis for the period 2017 to 2018 show a similar, albiet more smoothed, pattern (Fig. 6b, d; keep in mind that the spatial resolution of ERA5 is 30 km). There is strong heat loss along the cyclonic boundary current and in the
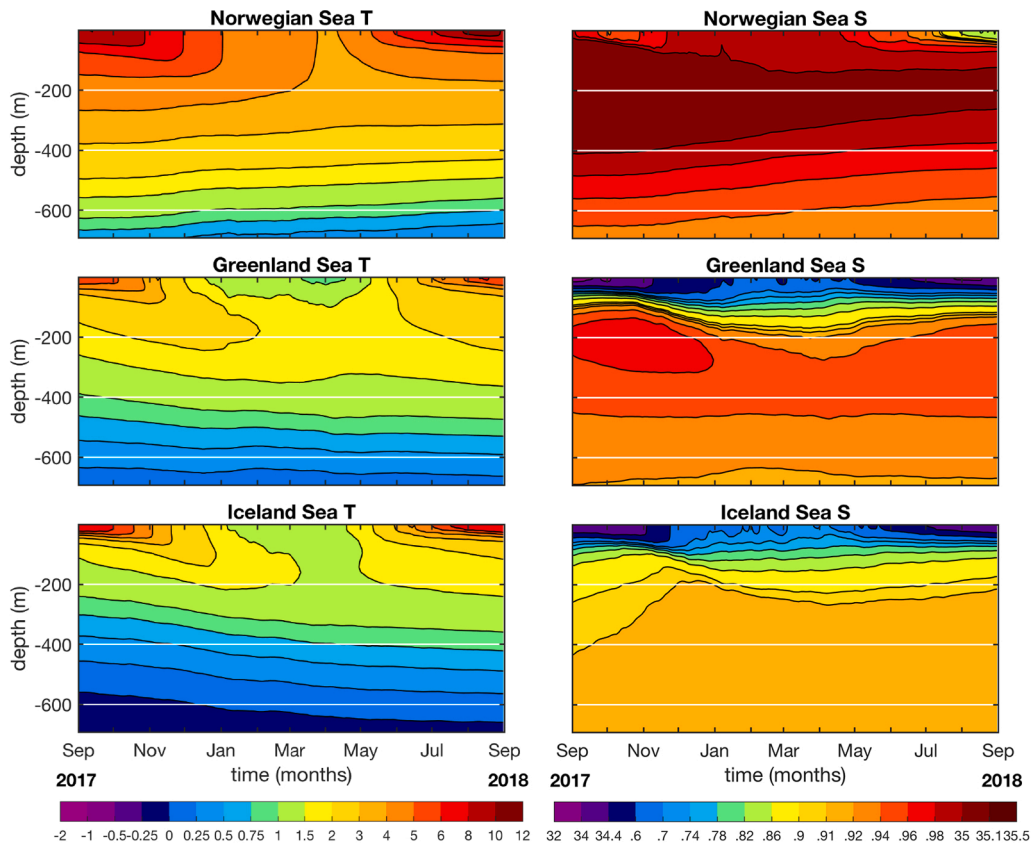
Table 1
Surface heat fluxes calculated for the Norwegian, Greenland, and Iceland Seas for the model and ERA5 for the year Sept 1, 2017 through Aug. 31, 2018. The annual mean surface heat flux is broken down into: total, inside mean gyres, outside gyres, ratio of inside to outside gyre. The area of the gyres in each basin and their sum are also given. The gyres as defined by the closed circulation contours shown in Fig. 6 and described in the text.

basin	total heat loss Q (10^{13} W)		inside gyre Q_g (10^{13} W)		outside gyre Q_o (10^{13} W)		ratio Q_g/Q_o		gyre area (10^{11} m^2)	
	model	ERA5	model	ERA5	model	ERA5	model	ERA5	model	climatology
Norwegian	3.6	5.9	1.1	1.9	2.5	4.0	0.43	0.47	4.1	3.0
Greenland	2.3	1.8	1.0	0.5	1.3	1.3	0.72	0.36	1.8	1.1
Iceland	0.67	0.48	0.04	0.09	0.63	0.39	0.06	0.23	0.73	0.65
Nordic	6.6	8.2	2.14	2.5	4.43	5.7	0.46	0.43	6.6	4.8

Fig. 5. Average model temperature (left column, °C) and salinity (right column, psu) in each of the basins as a function of depth and time. The basins are defined by the red lines in Fig. 1. The white lines are at constant depth in order to show more clearly the change in properties with time.
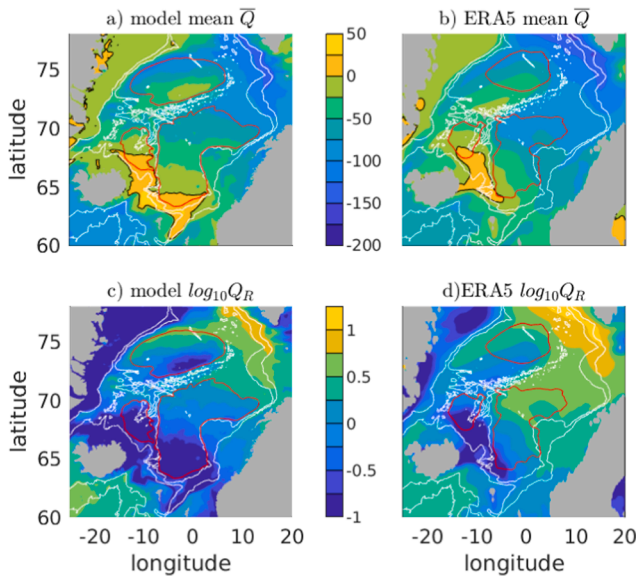

Fig. 6. Model a) annual mean surface heat flux $\overline{Q}$ (W/m², zero contour is in black); b)$log_{10} Q_R$, where Q_R is defined by (1). The red contours mark the outer limit of the model recirculation gyres and the white contours are the 1000 and 2000 m isobaths. c) and d) are the same quantities calculated from the ERA5 reanalysis for years 2017–2018, where the gyre boundaries are defined from the hydrographic climatology.

Norwegian Sea. The ERA5 reanalysis shows stronger heat loss over the central and southern Norwegian Sea because of the cold bias in the model. The reanalysis also shows a region of heat flux into the ocean just

north and east of Iceland, where the model has somewhat wider spread heat gain. There is more heat loss in the central and northern Norwegian Sea in the ERA5 reanalysis than in the model as well. Despite these differences, the model reproduces the same strong cooling over the cyclonic boundary current and the weaker heat loss in the interior of the Greenland and Iceland Seas. The Q_R from ERA5 shows a similar dominance of advection around the periphery of the basins and local atmospheric heating in the southern Greenland, Iceland, and Norwegian Seas for the seasonal restratification, as found in the model. ERA5 shows advection being stronger across the northern Norwegian Sea, again likely related to the model cold bias.

5. Advection between basins

In order to highlight the depth- and time-dependence of advection on the evolution of temperature and salinity within each of the basins, the advective tendency is defined relative to the basin-averaged property as a function of depth and time. The tendency is calculated through each of the sections shown in Fig. 1, where the along-track coordinate is *s* and the velocity normal to the section at depth level *k*, positive directed inward, is V_k.

$$\frac{\partial T_k}{\partial t} = \int V_k \left(T_k \left(s, z, t \right) - \overline{T}_k \left(z, t \right) \right) \Delta z_k \ ds \bigg/ VOL, \tag{2a}$$

$$\frac{\partial S_k}{\partial t} = \int V_k \left(S_k \left(s, z, t \right) - \overline{S}_k \left(z, t \right) \right) \Delta z_k \ ds \bigg/ VOL. \tag{2b}$$

The vertical grid spacing for level *k* is Δz_k and *VOL* is the volume of the basin from the surface to depth 692.5 m, which captures the dominant inter-basin fluxes of temperature and salinity. The basin-averaged temperature and salinity, $\overline{T}(z, t)$ and $\overline{S}(z, t)$, are shown in Fig. 5. This

approach is best interpreted as the tendency for lateral advection to change the basin-averaged temperature and salinity. It is not the same as the advective flux divergence tendency because there may be vertical transport within the basin, which is not accurately represented in (2) because the reference temperature and salinity are functions of depth. However, if the same calculation is carried out with a constant reference temperature or salinity the advective tendency is dominated by either the seasonal cycle (in time) or the mean stratification (in depth). The advantage of the present approach is that these effects are removed, so the tendencies are indicating how advection is changing the properties of the basin at that time and depth.

5.1. Mean advective tendencies

The cumulative tendencies as a function of depth and distance show where the heat and salt exchanges take place between the basins and higher/lower latitudes (Fig. 7). Regions where the tendency changes rapidly with distance are the locations where the fluxes enter/leave the basin. We show the cumulative tendency, rather than the tendency, because the integral along the sections results in smoother fields that more clearly demonstrate where exchange is taking place. Each section starts at the open white circle located at −7°W, 71.3°N in Fig. 1 and proceeds counterclockwise around each basin. The colored lines in Fig. 7 indicate the distance along the section that corresponds to the colored circles in Fig. 1.

The Norwegian Sea gains heat at the eastern side of the southern boundary from the surface down to 400 m from the Norwegian Atlantic Slope Current. This current also carries salty water below 100 m but anomalously fresh water in the upper 100 m, likely due to runoff from Norway to the south and perhaps low salinity water advected eastward from the north Icelandic shelf. There is little heat exchange through the eastern boundary, although the upper ocean does freshen along the coast. At the northern boundary the Norwegian Sea warms a little in the near surface due to the export of cold water but cools and freshens throughout the rest of the water column, especially below 200 m, along its western boundary with the Greenland Sea.

The Greenland Sea gains heat throughout the water column along its eastern boundary with the Norwegian Sea, while it gains salt mainly in the upper 100 m. The irregular nature of the advective fluxes along this section are likely due to aliasing of individual eddies that are shed from the frontal current along the ridge system, which are large but infrequent. The deep Greenland Sea warms along the northern boundary but the upper 100 m cools and freshens along the western end of this section due to the inflow of Arctic-origin waters. There is little change along the western boundary due to exchanges with the east Greenland shelf (it is demonstrated below that the seasonal signal is large even though the annual mean is small), while the export of warm, fresh waters to the south cools and salinifies the basin slightly.

The Iceland Sea imports cold, fresh water near the surface, and warm water below 100 m, from the north. There is little change along the western and southern boundaries while there is a large influx of heat, and some salt, below 100 m from the east (distance greater than 2000 km).

5.2. Mean and eddy decomposition

These advective influences can be further decomposed into mean and eddy fluxes, where the mean is taken as the time average and the eddy is perturbations relative to the time mean. The time series were summed in the vertical so the net influences of advection through each of the basin boundaries can be summarized in a single graph (Fig. 8). For each section the advective influence is presented as the mean contribution (on the left) and the eddy contribution (on the right). The Norwegian Sea is warmed by mean advection from the south and cooled primarily by both mean and eddy advection to the west and heat loss to the atmosphere. The sum of all these bars leads to a net cooling over the year, as reflected in the depth-time basin-averaged temperature in Fig. 5. The salinity in the Norwegian Sea is increased by advection from the south and decreased by both mean and eddy fluxes through each of the other boundaries, although the dominant loss is by mean advection to the west.

The Greenland sea imports heat and salt from the east, with both mean and eddy contributions being important. The heat is lost primarily to the atmosphere while salinity is reduced by mean advection from the
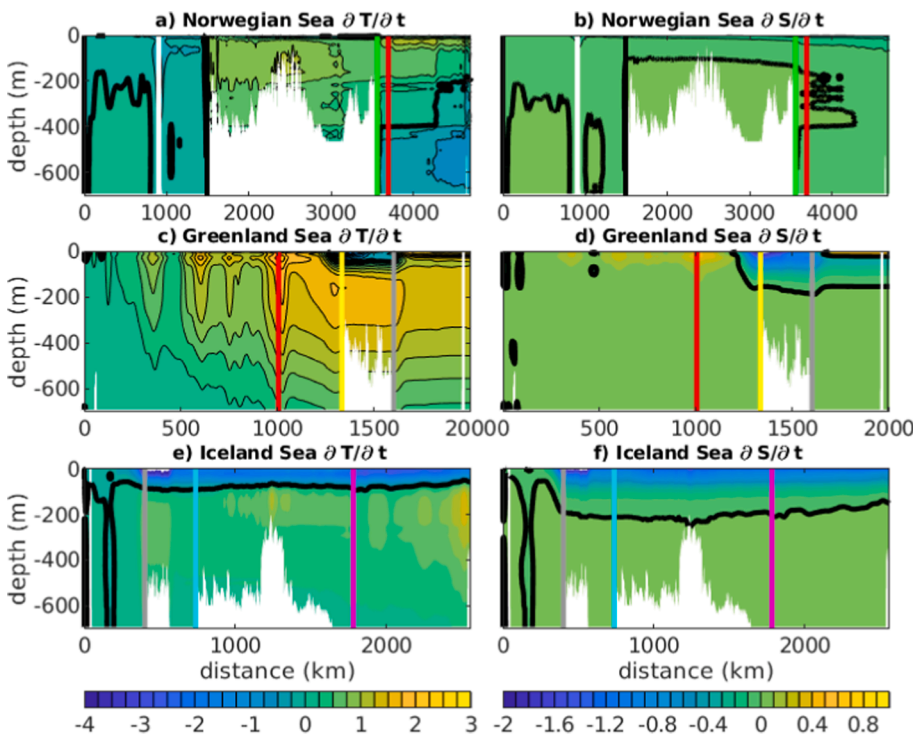

Fig. 7. Temperature (left column, °C/yr) and salinity (right column, psu/yr) tendencies as a function of depth and distance around each basin. Each section starts at the white circle in Fig. 1 and proceeds counterclockwise. The colored bars correspond to the colored dots on Fig. 1. The quantity plotted is the cumulative sum of the advective tendency at each depth. Regions of strong horizontal gradients are the locations where advection is changing the basin-averaged properties. The bold black line is the zero contour and white regions are topography.
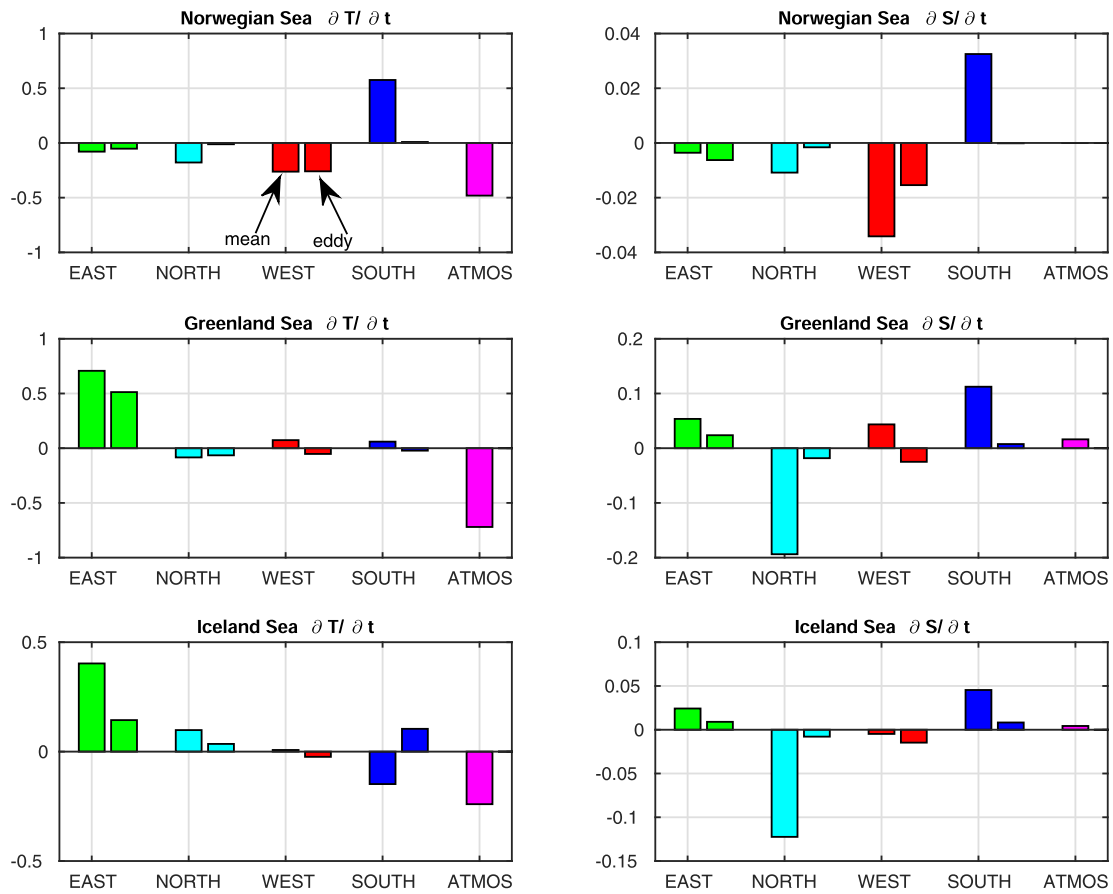
Fig. 8. Depth- and time-averaged model tendencies due to lateral advection and atmospheric forcing for temperature (left panels, $°C/yr$) and salinity (right panels, psu/yr) in each basin. The advective tendencies have been decomposed into mean (left bar) and eddy (right bar) contributions. The colors correspond to the side of the sea through which the advection occurs, consistent with Fig. 9.
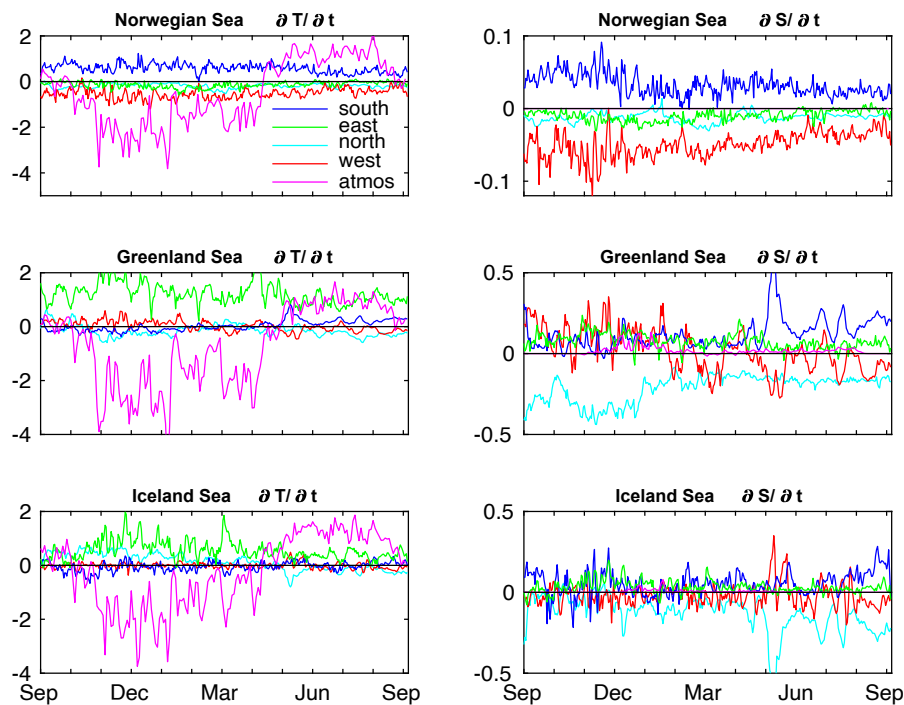

Fig. 9. Time series of the model depth-averaged advective temperature (left column, $°C/yr$) and salinity (right column, psu/yr) tendencies and surface forcing as a function of time. The colors correspond to the side of the basin, as defined in Fig. 1.

north. The increase in salinity due to advection through the southern boundary is driven by the export of water fresher, on average, than the Greenland Sea as a whole. The Iceland Sea shows a very similar profile with heat and salt imported from the east, atmospheric cooling, and freshwater imported from the north and exported to the south. Mean advection is as large or larger than eddy fluxes all across the Nordic Seas, emphasizing the importance of the cyclonic boundary current system in the lateral redistribution of heat and salt. Within the closed gyres the net heat loss to the atmosphere is balanced by lateral eddy fluxes (not shown), although it is ultimately mean advection that supplies the heat along the cyclonic boundary current system that then spawns the eddies.

5.3. Time dependence

The advective tendencies integrated in depth and around each of the basins are plotted in Fig. 9 as a function of time. The contributions are broken down into influences from the south, east, north, west, and atmospheric forcing. The location and depth of these inter-basin exchanges are shown in Fig. 7. The Norwegian Sea is made warmer and saltier by advection of Atlantic Water from the south. The seasonal variability in this advective tendency is relatively small, especially for temperature. The basin is cooled by exporting warm, salty water to the west, nearly in phase with the influence from the south. The basin is also cooled and freshened by exporting water to the north, although the influence is much less than the exchange to the west. Heat loss to the atmosphere is strong in the winter, partially offset by weaker warming in the summer. Surface forcing is negligible for salinity.

The Greenland Sea is made warmer and saltier by advection through its eastern boundary, this is some of the water that was exported to the west from the Norwegian Sea. Other advective influences for temperature are much smaller than this import from the east. Although there is a weak net cooling from the north, the tendency is strongly depth-dependent with strong cooling over the upper 100 m and weaker heating between 100 m and 700 m. These are the influences of Polar Water and recirculated Atlantic Water, respectively. The warming tendency is largely offset by heat loss to the atmosphere from October through May. The salinity is decreased by advection from the north. This is the influence of fresh waters exported from the Arctic. Some of this is then exported to the south. There is a seasonal signal in the salinity influence from the west, with increasing salinity in winter and decreasing salinity in summer. There is a small increase in salinity from surface forcing in winter due to brine rejection when ice forms in the western Greenland basin.

There is a major event in May that increases the salinity of the Greenland Sea by advection through the southern boundary. There is a corresponding decreasing tendency in the Iceland Sea. This is the signature of an export of a large region of low salinity water in the upper 100 m from the Greenland Sea into the Iceland Sea. It is nearly coincident with a large decrease in salinity coming from the western shelf in the Greenland Sea. However, this large flux from the west is not the only such event and this section is dominated by distinct, large amplitude

events throughout the year. A comparison between the salinity tendency of the Greenland Sea from the west and the wind stress to the northeast, averaged within 3 degrees longitude of the 650 m isobath, shows that when the wind is strong and to the southwest the salt flux across the 650 m isobath tends to increase the salinity of the Greenland Sea and when winds are weaker than normal or to the northeast the flux tends to decrease the salinity in the Greenland Sea (Fig. 10). The two time series are correlated at −0.50, which is statistically significant at greater than 95%. This is consistent with a rapid response to the Ekman transport: winds towards the southwest will have an onshore Ekman transport and advect low salinity water towards the coast, increasing the salinity in the interior, while winds towards the northeast will advect low salinity water off the shelf. Våge et al. (2018) demonstrated that, on the seasonal timescale, this process impacts the ventilation of water in the East Greenland Current. Weak winds also correspond to freshening periods because it is not just an active Ekman transport that carries low salinity water offshore. The East Greenland Current is baroclinically unstable and eddies act to transport low salinity water offshore. Ekman transport during periods of southwest winds oppose this offshore flux but during periods of weak wind the eddies are able to progress offshore. Most of this offshore flux occurs in the southern Greenland Sea, close to the Iceland Sea. This mechanism was also proposed as a means to flux low salinity water offshore near the Blosseville Basin (69 °N) and form the Separated East Greenland Current (Våge et al., 2013), although in that case the change in wind was due to a change in the coastal orientation rather than time-dependence. This offshore flux of low salinity water is also connected to advection from the Greenland Sea into the Iceland Sea. The low-salinity water is advected to the south in the form of meanders of the East Greenland Current, mesoscale eddies, and smaller-scale filaments. The correlation between the salinity tendency from the west and the export to the south is −0.53 and the strongest correlation is found when the salinity tendency from the west leads that to the south by 4 days. So while the mean salinity tendency from the shelf into the interior of the Greenland Sea is small (0.019 psu/yr), the offshore flux of low salinity water in summer is rapidly exported to the south, indicating the importance of this wind-driven exchange to the stratification of the larger region.

The Iceland Sea is also warmed and made saltier from the east and made fresher from the north, similar to the Greenland Sea. It is also made slightly warmer from the north, which is due to the recirculated Atlantic Water. Heat loss to the atmosphere is the dominant source of cooling in the Iceland basin.

6. Summary

The Nordic Seas are a key region for water mass transformation and the downwelling limb of the meridional overturning circulation. The circulation is dominated by a cyclonic boundary current system and closed recirculation gyres within the Norwegian, Greenland, and Iceland Seas. Warm, salty water is advected from the south while cold, fresh water is advected from the north. Understanding the means by which
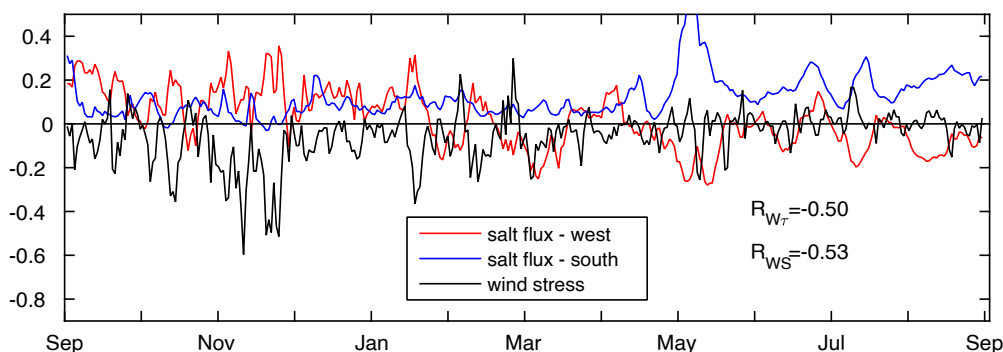

Fig. 10. Time series of model daily average wind stress parallel to the 650 m isobath in the western Greenland Sea between 72 °N and 77 °N (black line, positive to the northeast, N/m^2); the salt flux tendency across the 650 m isobath (red line from Fig. 9, psu/yr); and the salt flux tendency due to advection into the Iceland Sea (blue line from Fig. 9, psu/yr). The correlation between the flux across the 650 m isobath and: the wind ($R_{W\tau}$) is −0.50; the flux into the Iceland Sea (R_{WS}) is −0.53 when the flux lags the wind by 4 days.

heat and salt are redistributed and balance air-sea fluxes is essential for understanding the general circulation, hydrography, and water mass transformation within the Nordic Seas.

A regional, high-resolution coupled sea ice - ocean model and a hydrographic climatology were used to assess the mean state and seasonal cycle within the Norwegian, Greenland, and Iceland Seas. Although the model has biases, it reproduces the major water masses and currents in the region and so provides a useful tool with which to investigate lateral advection of heat and salt that is not possible with the spatially and temporally limited direct observations. Air-sea heat flux was used to infer that lateral advection dominates the seasonal cycle in temperature in the cyclonic boundary current system, particularly in the northern Norwegian and Greenland Seas. On the other hand, local air-sea exchange dominates over lateral advection for the seasonal cycle within the closed recirculation gyres and across the southern Nordic Seas.

There is strong heating of the Norwegian Sea from the south and a freshening of the Greenland Sea from the north. The heat flux into the Norwegian Sea is redistributed within the Nordic Seas and lost to the atmosphere locally within the Norwegian Sea. The freshwater imported from the north is partially exported to the south and partially balanced by the import of salty waters into the Norwegian Sea that is then redistributed across the Nordic Seas. The dominant exchange between the basins is a westward flux of warm, salty water from the Norwegian Sea into the Greenland and Iceland Seas, with approximately 50% due to mean advection and 50% due to eddy fluxes. This westward flux may be too strong in the model, however, since the model Norwegian Sea is slightly cooler, and the Greenland Sea is warmer, than in the climatology. The recirculated Atlantic Water along the western side of the Greenland Sea in the model is also too warm and salty compared to climatological observations. This warm bias may be a result of too little heat loss in the Norwegian Sea, which appears to be related to low salinity water spreading eastward from the north Icelandic shelf. It is difficult to determine how much of this stratification bias in the Greenland Sea is due to the relatively mild winter of 2017/2018, as documented by Renfrew et al. (2019), and how much is due to bias in the model.

The exchange between the Greenland Sea and the east Greenland Shelf is largely controlled by winds. During winter, when the winds are often strong and towards the southwest, the Ekman transport advects low salinity water onto the shelf, leading to an increasing tendency for the salinity of the Greenland Sea. During summer, when the winds are weak or towards the northeast, this freshwater is fluxed across the shelfbreak by eddies and leads to a freshening of the Greenland Sea. This exchange takes place predominantly in the southern Greenland Sea, where the anomalous water is quickly advected into the Iceland Sea.

These results emphasize the importance of the exchange between the basins within the Nordic Seas for balancing surface heat loss and freshwater runoff, and in determining the properties of the waters that are exported to the south. Both mean and eddy advection are important, with mean advection dominating within the cyclonic boundary current and eddy fluxes dominating within the closed recirculation gyres. Approximately 2/3 of the total heat loss occurs over the cyclonic boundary current and 1/3 occurs within the regions of the closed recirculation gyres in both the numerical model and the ERA5 reanalysis.

Declaration of Competing Interest

The authors declare that they have no known competing financial interests or personal relationships that could have appeared to influence the work reported in this paper.

Acknowledgments

References

Aagaard, K., Swift, J., Carmack, E., 1985. Thermohaline circulation in the Arctic Mediterranean Seas. J. Geophys. Res. 90, 4833–4846.

Adcroft, A., Campin, J.-M., Hill, C., Marshall, J., 2004. Implementation of an Atmosphere-Ocean General Circulation Model on the Expanded Spherical Cube. Mon. Weather Rev. 132 (12), 2845–2863. https://doi.org/10.1175/MWR2823.1.

Almansi, M., Gelderloos, R., Haine, T., Saberi, A., Siddiqui, A., 2019. OceanSpy: A Python package to facilitate ocean model data analysis and visualization. J. Open Source Softw. 4 (39), 1506. https://doi.org/10.21105/joss.01506 http://joss.theoj.org/papers/10.21105/joss.01506.

Almansi, M., Haine, T.W.N., Gelderloos, R., Pickart, R.S., 2020. Evolution of Denmark Strait Overflow Cyclones and Their Relationship to Overflow Surges. Geophys. Res. Lett. 47 (4) https://doi.org/10.1029/2019gl086759 https://agupubs.onlinelibrary.wiley.com/doi/abs/10.1029/2019GL086759.

Almansi, M., Haine, T.W.N., Pickart, R.S., Magaldi, M.G., Gelderloos, R., Mastropole, D., 2017. High-frequency variability in the circulation and hydrography of the denmark strait overflow from a high-resolution numerical model. J. Phys. Oceanogr. 47 (12), 2999–3013. https://doi.org/10.1175/JPO-D-17-0129.1.

Årthun, M., Eldevik, T., 2016. On Anomalous Ocean Heat Transport toward the Arctic and Associated Climate Predictability. J. Climate 29, 689–704.

Borenäs, K., Lundberg, P., 2004. The Faroe-Bank Channel deep-water overflow. Deep-Sea Res. Part II: Top. Stud. Oceanogr. 51 (4–5), 335–350. https://doi.org/10.1016/j.dsr2.2003.05.002. http://www.sciencedirect.com/science/article/pii/S0967064504000244.

Brakstad, A., Våge, K., Håvik, L., MOORE, G.W., 2019. Water mass transformation in the Greenland sea during the period 1986–2016. J. Phys. Oceanogr. 49 (1), 121–140. https://doi.org/10.1175/JPO-D-17-0273.1.

Campin, J.-M., Adcroft, A., Hill, C., Marshall, J., 2004. Conservation of properties in a free-surface model. Ocean Model. 6 (3), 221–244. https://doi.org/10.1016/S1463-5003(03)00009-X. http://www.sciencedirect.com/science/article/pii/S1463500300009X.

Casanova-Masjoan, M. et al., 2020: Alongstream, seasonal and interannual variability of the north icelandic irminger current and east icelandic current around iceland. J. Geophys. Res.: Oceans, e2020JC016283, doi: 10.1029/2020JC016283, https://agupubs.onlinelibrary.wiley.com/doi/abs/10.1029/2020JC016283.

Chafik, L., Rossby, T., 2019. Volume, Heat, and Freshwater Divergences in the Subpolar North Atlantic Suggest the Nordic Seas as Key to the State of the Meridional Overturning Circulation. Geophys. Res. Lett. 46 (9), 4799–4808. https://doi.org/10.1029/2019GL082110 https://agupubs.onlinelibrary.wiley.com/doi/abs/10.1029/2019GL082110.

Copernicus Climate Change Service (C3S), 2017. RA5: Fifth generation of ECMWF atmospheric reanalyses of the global climate. Copernicus Climate Change Service Climate Data Store (CDS). European Centre for Medium-Range Weather Forecasts. https://cds.climate.copernicus.eu/cdsapp#!/home.

Cummings, J.A., 2005. Operational multivariate ocean data assimilation. Quart. J. Roy. Meteorol. Soc. 131 (613), 3583–3604. https://doi.org/10.1256/qj.05.105 https://rmets.onlinelibrary.wiley.com/doi/abs/10.1256/qj.05.105, https://rmets.onlinelibrary.wiley.com/doi/pdf/10.1256/qj.05.105.

Cummings, J.A., Smedstad, O.M., 2013. Variational Data Assimilation for the Global Ocean, 303–343. Springer Berlin Heidelberg, Berlin, Heidelberg, doi: 10.1007/978-3-642-35088-7_13, URL https://doi.org/10.1007/978-3-642-35088-7_13.

Dickson, R.R., Brown, J., 1994. The production of North Atlantic Deep Water: sources, rates and pathways. J. Geophys. Res. 99, 12 319–12 341.

Donlon, C.J., Martin, M., Stark, J., Roberts-Jones, J., Fiedler, E., Wimmer, W., 2012. The Operational Sea Surface Temperature and Sea Ice Analysis (OSTIA) system. Remote Sens. Environ. 116, 140–158. https://doi.org/10.1016/j.rse.2010.10.017. http://www.sciencedirect.com/science/article/pii/S0034425711002197.

Eldevik, T., Nilsen, J.E.Ø., Iovino, D., Olsson, K.A., Sandø, A., Drange, H., 2009. Observed sources and variability of nordic seas overflow. Nat. Geosci. 2, 406–410. https://doi.org/10.1038/NGEO518.

Hansen, B., Husgaro, K.M., Hátún, H., Østerhus, S., 2016. A stable Faroe Bank Channel overflow 1995–2015. Ocean Sci. 12 (6), 1205–1220. https://doi.org/10.5194/os-12-1205-2016. https://www.ocean-sci.net/12/1205/2016/.

Hansen, B., Østerhus, S., 2000. North Atlantic-Nordic Seas exchanges. Prog. Oceanogr. 45, 109–208 doi:PII:S00 79-6611(99)00052-X.

Harden, B.E., et al., 2016. Upstream sources of the Denmark Strait Overflow: Observations from a high-resolution mooring array. Deep Sea Res. 112, 94–112. https://doi.org/10.1016/j.dsr.2016.02.007.

Helber, R.W., Townsend, T.L., Barron, C.N., Dastugue, J.M., Carnes, M.R., 2013. Validation test report for the improved synthetic ocean profile (isop) system, part i: Synthetic profile methods and algorithm. Tech. rep. Naval Research Lab Stennis Detachment Stennis Space Center MS Oceanography Div.

Helland-Hansen, B., Nansen, F., 1909. The Norwegian Sea: its physical oceanography based upon the Norwegian researches 1900–1904. Det Mallingske Bogtrykkeri.

Huang, J., Pickart, R.S., Huang, R.X., Lin, P., Brakstad, A., Xu, F., 2020. Sources and upstream pathways of the densest overflow water in the Nordic Seas. Nat. Commun. 11 (1), 5389.

Ingvaldsen, R., Loeng, H., Asplin, L., 2002. Variability in the Atlantic inflow to the Barents Sea based on a one-year time series from moored current meters. Cont. Shelf Res. 22, 505–519.

Jakobsen, P.K., Ribergaard, M.H., Quadfasel, D., Schmith, T., Hughes, C.W., 2003. Near-surface circulation in the northern North Atlantic as inferred from Lagrangian drifters: Variability from the mesoscale to interannual. J. Geophys. Res. Oceans 108 (8), 1–14. https://doi.org/10.1029/2002jc001554 https://agupubs.onlinelibrary. wiley.com/doi/abs/10.1029/2002JC001554.

Jónsson, S., Valdimarsson, H., 2012. Water mass transport variability to the North Icelandic shelf, 1994–2010. ICES J. Mar. Sci. 69 (5), 809–815. https://doi.org/ 10.1093/icesjms/fss024. https://academic.oup.com/icesjms/article-pdf/69/5/809/ 29145177/fss024.pdf.

Jochumsen, K., Moritz, M., Nunes, N., Quadfasel, D., Larsen, K.M., Hansen, B., Valdimarsson, H., Jonsson, S., 2017. Revised transport estimates of the Denmark Strait overflow. J. Geophys. Res. Oceans 122 (4), 3434–3450. https://doi.org/ 10.1002/2017JC012803 https://agupubs.onlinelibrary.wiley.com/doi/abs/ 10.1002/2017JC012803.

Jónsson, S., Valdimarsson, H., 2004. A new path for the Denmark Strait overflow water from the Iceland Sea to Denmark Strait. Geophys. Res. Lett. 31 (L03), 305. https:// doi.org/10.1029/2003GL019214.

Large, W.G., McWilliams, J.C., Doney, S.C., 1994. Oceanic vertical mixing: A review and a model with a nonlocal boundary layer parameterization. Rev. Geophys. 32, 363–403.

Latarius, K., Quadfasel, D., 2016. Water mass transformation in the deep basins of the nordic seas: Analyses of heat and freshwater budgets. Deep Sea Res. I 114, 23–42. https://doi.org/10.1016/j.dsr.2016.04.012.

Lin, P., Pickart, R., Jochumsen, K., Moore, G., Valdimarsson, H., Fristedt, T., Pratt, L.J., 2020. Kinematic Structure and Dynamics of the Denmark Strait Overflow from Ship-based Observations. J. Phys. Oceanogr. doi: 10.1175/JPO-D-20-0095.1 (in press).

Losch, M., Menemenlis, D., Campin, J.M., Heimbach, P., Hill, C., 2010. On the formulation of sea-ice models. Part 1: Effects of different solver implementations and parameterizations. Ocean Model. 33 (1), 129–144. https://doi.org/10.1016/j. ocemod.2009.12.008. http://www.sciencedirect.com/science/article/pii/S1463500 309002418.

Marshall, J., Hill, C., Perelman, L., Adcroft, A., 1997. Hydrostatic, quasi-hydrostatic, and non-hydrostatic ocean modeling. J. Geophys. Res. 102, 5733–5752.

Mauritzen, C., 1996a. Production of dense overflow waters feeding the North Atlantic across the Greenland-Scotland Ridge. Evidence for a revised circulation scheme. Deep Sea Res. 43, 769–806. https://doi.org/10.1016/0967-0637(96)00037-4.

Mauritzen, C., 1996b. Production of dense overflow waters feeding the North Atlantic across the Greenland-Scotland Ridge. Part 2: An inverse model. Deep Sea Res. 43, 807–835.

Mauritzen, C., et al., 2011. Closing the loop – approaches to monitoring the state of the arctic mediterranean during the international polar year 2007–2008. Prog. Oceanogr. 90 (1), 62–89. https://doi.org/10.1016/j.pocean.2011.02.010. http:// www.sciencedirect.com/science/article/pii/S0079661111000255, arctic Marine Ecosystems in an Era of Rapid Climate Change.

McDougall, T.J., Jackett, D.R., Wright, D.G., Feistel, R., 2003. Accurate and computationally efficient algorithms for potential temperature and density of seawater. J. Atmos. Oceanic Technol. 20 (5), 730–741. https://doi.org/10.1175/ 1520-0426(2003)20<730:AACEAF%3E2.0.CO;2.

Medvedev, D., Lemson, G., Rippin, M., 2016. SciServer Compute: Bringing Analysis Close to the Data. In: Proceedings of the 28th International Conference on Scientific and Statistical Database Management, ACM, Budapest, Hungary, 27:1–27:4, doi: 10.1145/2949689.2949700, URL http://doi.acm.org/10.1145/2949689.2949700.

Oliver, K.I.C., Heywood, K.J., 2003. Heat and Freshwater Fluxes through the Nordic Seas. J. Phys. Oceanogr. 33, 1009–1026.

Orvik, K.A., Niiler, P., 2002. Major pathways of Atlantic water in the northern North Atlantic and Nordic Seas toward Arctic. Geophys. Res. Lett. 29 (19), 1–4. https://doi. org/10.1029/2002GL015002 https://agupubs.onlinelibrary.wiley.com/doi/abs/ 10.1029/2002GL015002.

Orvik, K.A., Skagseth, Ø., Mork, M., 2001. Atlantic inflow to the Nordic Seas: current structure and volume fluxes from moored current meters, VM-ADCP and SeaSoar-CTD observations, 1995–1999. Deep-Sea Part I 48, 937–957. https://doi.org/ 10.1029/2002/GL015002.

Østerhus, S., et al., 2019. Arctic Mediterranean exchanges: a consistent volume budget and trends in transports from two decades of observations. Ocean Sci. 15, 379–399. https://doi.org/10.5194/os-15-379-2019.

Perkins, H., Hopkins, T.S., Malmberg, S.-A., Poulain, P.-M., Warn-Varnas, A., 1998. Oceanographic conditions east of iceland. J. Geophys. Res. 103, 21 531–21 542.

Pickart, R.S., Smethie, W.M., 1998. Temporal evolution of the deep western boundary current where it enters the subtropical domain. Deep Sea Res. I 45, 1053–1083.

Poulain, P.-M., Warn-Varnas, A., Niiler, P.P., 1996: Near-surface circulation of the Nordic seas as measured by Lagrangian drifters. J. Geophys. Res.: Oceans 101 (C8), 18237–18258. doi: 10.1029/96JC00506. https://agupubs.onlinelibrary.wiley.com/ doi/abs/10.1029/96JC00506.

Price, J.F., Baringer, M.O., 1994. Outflows and deep water production by marginal seas. Prog. Oceanogr. 33, 161–200.

Renfrew, I.A., et al., 2019. The Iceland Greenland Seas Project. Bull. Am. Meteorol. Soc. 100 (9), 1795–1817. https://doi.org/10.1175/BAMS-D-18-0217.1. https://journals. ametsoc.org/bams/article-pdf/100/9/1795/4871780/bams-d-18-0217_1.pdf.

Schaffer, J. et al., 2019. An update to Greenland and Antarctic ice sheet topography, cavity geometry, and global bathymetry (RTopo-2.0.4). PANGAEA, doi: 10.1594/ PANGAEA.905295, supplement to: Schaffer, Janin; Kanzow, Torsten; von Appen, Wilken-Jon; von Albedyll, Luisa; Arndt, Jan Erik; Roberts, David H (2020): Bathymetry constrains ocean heat supply to Greenland's largest glacier tongue. Nat. Geosci. 13(3), 227-231. https://doi.org/10.1038/s41561-019-0529-x, doi:10.1594/ PANGAEA.905295.

Schlochtholz, P., 2013. Observational evidence for oceanic forcing of atmospheric variability in the nordic seas area. J. Climate 26, 2957–2975.

Segtnan, O.H., Furevik, T., Jenkins, A.D., 2011. Heat and freshwater budgets of the Nordic seas computed from atmospheric reanalysis and ocean observations. J. Geophys. Res.: Oceans 116 (11), 1–17. https://doi.org/10.1029/2011JC006939 https://agupubs.onlinelibrary.wiley.com/doi/abs/10.1029/2011JC006939.

Semper, S., Våge, K., Pickart, R.S., Valdimarsson, H., Torres, D.J., Jónsson, S., 2019. The emergence of the North Icelandic Jet and its evolution from northeast Iceland to Denmark Strait. J. Phys. Oceanogr. 49 (10), 2499–2521. https://doi.org/10.1175/ JPO-D-19-0088.1.

Semper, S., Pickart, R.S., Våge, K., et al., 2020. The Iceland-Faroe Slope Jet: a conduit for dense water toward the Faroe Bank Channel overflow. Nat. Commun. 11, 5390. https://doi.org/10.1038/s41467-020-19049-5.

Simonsen, K., Haugan, P.M., 1996. Heat budgets of the Arctic Mediterranean and sea surface heat flux parameterizations for the Nordic Seas. J. Geophys. Res. C: Oceans 101 (C3), 6553–6576. https://doi.org/10.1029/95JC03305 https://agupubs. onlinelibrary.wiley.com/doi/abs/10.1029/95JC03305.

Spall, M.A., 2010. Non-local topographic influences on deep convection: An idealized model for the nordic seas. Ocean Model. 32, 72–85.

Strass, V.H., Fahrbach, E., Schauer, U., Sellmann, L., 1993. Formation of Denmark Strait overflow water by mixing in the East Greenland Current. J. Geophys. Res.: Oceans 98 (C4), 6907–6919. https://doi.org/10.1029/92JC02732 https://agupubs. onlinelibrary.wiley.com/doi/abs/10.1029/92JC02732.

Swift, J., Aagaard, K., Malmberg, S.-A., 1980. The contribution of the Denmark Strait overflow to the deep North Atlantic. Deep Sea Res. 27, 29–42.

Våge, K., Papritz, L., Håvik, L., Spall, M.A., Moore, G., 2018. Ocean convection linked to the recent ice edge retreat along east Greenland. Nat. Comm. 9, 1287. https://doi. org/10.1038/s41467-018-03468-6.

Våge, K., Pickart, R.S., Spall, M.A., Moore, G.W.K., Valdimarsson, H., Torres, D.J., E.S.Y., Nilsen, J.E.Ø., 2013. Revised circulation scheme north of the Denmark Strait. Deep Sea Res. I, 79, 20–39. doi:10.1016/j.dsr.2013.05.007.

Våge, K., Pickart, R.S., Spall, M.A., Valdimarsson, H., Jónsson, S., Torres, D.J., Østerhus, S., Eldevik, T., 2011. Significant role of the North Icelandic Jet in the formation of Denmark Strait overflow water. Nat. Geosci. 4 (10), 723–727. https:// doi.org/10.1038/ngeo1234. https://domicile.ifremer.fr/ngeo/journal/v4/n10/full/ , DanaInfo=www.nature.com+ngeo1234.html.

Vöet, G., Quadfasel, D., Mork, K.A., Søiland, H., 2010. The mid-depth circulation of the Nordic Seas derived from profiling float observations. Tellus, Ser. A: Dyna. Meteorol. Oceanogr. 62 (4), 516–529. https://doi.org/10.1111/j.1600-0870.2010.00444.x https://www.tandfonline.com/doi/abs/10.1111/j.1600-0870.2009.00444.x.

Woodgate, R.A., Aagaard, K., Weingartner, T.J., 2006. Interannual changes in the Bering Strait fluxes of volume, heat and freshwater between 1991 and 2004. Geophys. Res. Lett. 33 (15), 2–6. https://doi.org/10.1029/2006GL026931 https://agupubs. onlinelibrary.wiley.com/doi/abs/10.1029/2006GL026931.

Woodgate, R.A., Weingartner, T.J., Lindsay, R., 2012. Observed increases in Bering Strait oceanic fluxes from the Pacific to the Arctic from 2001 to 2011 and their impacts on the Arctic Ocean water column. Geophys. Res. Lett. 39 https://doi.org/10.1029/ 2012GL054092.

Xie, J., Bertino, L., Counillon, F., Lisæter, K.A., Sakov, P., 2017. Quality assessment of the topaz4 reanalysis in the arctic over the period 1991–2013. Ocean Sci. 13 (1), 123–144. https://doi.org/10.5194/os-13-123-2017 https://os.copernicus.org/ articles/13/123/2017/.